How chains and rings affect the dynamic magnetic susceptibility of a highly clustered ferrofluid

How chains and rings affect the dynamic magnetic susceptibility of a highly clustered ferrofluid

Philip J. Camp*
School of Chemistry, University of Edinburgh, David Brewster Road, Edinburgh EH9 3FJ, Scotland and Department of Theoretical and Mathematical Physics, Institute of Natural Sciences and Mathematics, Ural Federal University, 51 Lenin Avenue, Ekaterinburg 620000, Russia

Alexey O. Ivanov
Department of Theoretical and Mathematical Physics, Ural Mathematical Center, Institute of Natural Sciences and Mathematics, Ural Federal University, 51 Lenin Avenue, Ekaterinburg 620000, Russia

Julien O. Sindt
EPCC, Bayes Centre, University of Edinburgh, 47 Potterrow, Edinburgh EH8 9BT, Scotland
(Dated: June 3, 2021)

The dynamic magnetic susceptibility, $\chi(\omega)$, of a model ferrofluid at very low concentration (volume fraction approximately 0.05%), and with a range of dipolar coupling constants ($1 \leq \lambda \leq 8$), is examined using Brownian dynamics simulations. With increasing λ, the structural motifs in the system change from unclustered particles, through chains, to rings. This gives rise to a nonmonotonic dependence of the static susceptibility $\chi(0)$ on λ, and qualitative changes to the frequency spectrum. The behavior of $\chi(0)$ is already understood, and the simulation results are compared to an existing theory. The single-particle rotational dynamics are characterized by the Brownian time, $\tau_{\rm B}$, which depends on particle size, carrier-liquid viscosity, and temperature. With $\lambda \leq 5.5$, the imaginary part of the spectrum, $\chi''(\omega)$, shows a single peak near $\omega \sim \tau_{\rm B}^{-1}$, characteristic of single particles. With $\lambda \geq 5.75$, the spectrum is dominated by the low-frequency response of chains. With $\lambda \geq 7$, new features appear at high frequency, which correspond to intracluster motions of dipoles within chains and rings. The peak frequency corresponding to these intracluster motions can be computed accurately using a simple theory.

I. INTRODUCTION

A fundamental property of a magnetic material is its response to an applied magnetic field. The ability to tune the electrical, optical, magnetic, rheological, and thermal properties of magnetic fluids with fields has led to manifold applications [1]. Magnetic fluids include colloidal suspensions of ferromagnetic or superparamagnetic particles in a nonmagnetic carrier liquid (ferrofluids). One important property is the dynamic response of the fluid magnetization to an ac magnetic field. If the field is weak, then the linear response is defined by the initial dynamic magnetic susceptibility, $\chi(\omega)$, which consists of real (in-phase, χ') and imaginary (out-of-phase, χ'') parts. Power dissipation is proportional to χ'' [2], and so magnetic fluids can be heated *in situ* to provide localized heating, such as in magnetic hyperthermia treatments of diseased tissue [3–7].

Many studies have been carried out to understand how material properties affect the dynamic magnetic susceptibility of magnetic fluids [8–10], and there continues to be a lot of activity in the area. The dynamics of non-interacting ferromagnetic particles are governed by the Brownian rotation mechanism [1], with a characteristic rotation time $\tau_{\rm B} = \pi\eta\sigma^3/2k_{\rm B}T$, where η is the carried-liquid viscosity, σ is the particle diameter, $k_{\rm B}$ is Boltzmann's constant, and T is the temperature. In this case, the magnetic response is known exactly, and the theoretical results can be applied to typical ferrofluids at low concentrations. The case of superparamagnetic particles introduces the complication of there being both Brownian rotation and Néel relaxation mechanisms [1, 11], and this is not considered here.

A lot of recent theoretical work has focused on the role of interactions between particles, which generally lead to an increase in the characteristic rotational timescales, due to correlations between particles in transient clusters. Consequently, the peak in χ'' – corresponding to maximum power dissipation – shifts to lower frequency. One of the most successful approaches is the dynamical modified mean field theory devised by Ivanov and co-workers [12], and subsequently tested against experimental measurements [13–15], and computer simulations [16]. An extension of this approach has been made to treat a combination of static and ac (probing) magnetic fields [17, 18]. The basic idea is that the local field experienced by a single particle is a superposition of the applied field(s), and the field due to the magnetization of the rest of the particles. The method for calculating the latter contribution is based on the Yvon-Born-Green equation, and well-controlled approximations for the pair distribution function, from statistical mechanics [19]. Improvements have been proposed and tested re-

* Corresponding author: philip.camp@ed.ac.uk

cently [20], but the applicability of the theory is limited to the regime where there is no extensive clustering of particles into chains and rings.

The extent of clustering is mainly controlled by the interaction strength, characterized by the dipolar coupling constant $\lambda = \mu_0\mu^2/4\pi\sigma^3 k_\mathrm{B}T$, where μ_0 is the vacuum permeability, and μ is the magnitude of the magnetic dipole moment on a particle. Roughly speaking, cluster formation is favored when $\lambda \gtrsim 4$ [21–25]. The focus of this work is the large-λ, low-concentration regime, where chains and rings are the predominant, self-assembled structural motifs [26–29]. The initial static magnetic susceptibility has been shown to be highly sensitive to the formation of such clusters [30]. At low concentration and high temperature (low λ), the particles are unclustered, and the static susceptibility is close to the Langevin susceptibility for noninteracting particles. As the temperature is decreased (λ is increased), chains form, and this increases the susceptibility above the Langevin value because the chains possess large net magnetic moments. Eventually, the chains close up to form rings, and since these have negligible net moments, the susceptibility decreases below the Langevin value. The net result is a nonmonotonic dependence of the susceptibility on λ.

The structure and dynamics in the highly structured regime have been surveyed comprehensively using computer simulations, and strong effects of cluster formation on the diffusion coefficient, viscosity, and intermediate scattering function have been uncovered [31]. The aim of the current work is to demonstrate the effects of clusters on the dynamic magnetic response, using Brownian-dynamics (BD) simulations, and analytical theory. Clusters give rise to new complexity in $\chi(\omega)$, with a range of characteristic timescales arising from a mixture of single-particle rotations, chain rotations, and motions of particles within chains and rings.

The rest of this article is organized as follows. The model and methods are detailed in Section II, including the basic model parameters (Section II A), the BD simulation protocol (Section II B), and a theory of the static susceptibility (Section II C). Section III contains the results for the static susceptibility (Section III A), the dynamic susceptibility (III B), and a theory of the high-frequency dynamic response (III C). Section IV concludes the article.

II. MODEL AND METHODS

A. Model

The ferrofluid is modeled as a system of N spherical particles confined to a volume V, and at temperature T. Each particle carries a central, point dipole moment $\boldsymbol{\mu}$. The interaction between dipoles is given by

$$u_{ij}^\mathrm{d} = \frac{\mu_0}{4\pi}\left[\frac{(\boldsymbol{\mu}_i\cdot\boldsymbol{\mu}_j)}{r_{ij}^3} - \frac{3\,(\boldsymbol{\mu}_i\cdot\boldsymbol{r}_{ij})\,(\boldsymbol{\mu}_j\cdot\boldsymbol{r}_{ij})}{r_{ij}^5}\right] \quad (1)$$

where μ_0 is the vacuum permeability, $\boldsymbol{r}_i$ is the position vector of particle i, and $\boldsymbol{r}_{ij} = \boldsymbol{r}_j - \boldsymbol{r}_i$ is the separation vector between particles i and j. In the BD simulations (Section II B), the short-range, nonmagnetic interaction is given by the Weeks-Chandler-Andersen (WCA) potential

$$u_{ij}^\mathrm{WCA} = \begin{cases} 4\epsilon\left[\left(\frac{\sigma}{r}\right)^{12} - \left(\frac{\sigma}{r}\right)^{6}\right] + \epsilon & r \le r_\mathrm{m} \\ 0 & r > r_\mathrm{m} \end{cases} \quad (2)$$

where ϵ and σ are the Lennard-Jones energy and diameter parameters, respectively, and $r_\mathrm{m} = 2^{1/6}\sigma$ is the position of the minimum in the Lennard-Jones potential. The temperature is fixed so that $T^* = k_\mathrm{B}T/\epsilon = 1$. In the theoretical treatment of the static susceptibility (Section II C), it is more convenient to consider hard-sphere particles with diameter σ. In any case, the dipolar coupling constant is defined as $\lambda = \mu_0\mu^2/4\pi\sigma^3 k_\mathrm{B}T$, where k_B is Boltzmann's constant, the reduced concentration is $\rho\sigma^3 = N\sigma^3/V$, and the volume fraction is $\varphi = \pi\rho\sigma^3/6$. This work is focused on a single concentration of $\rho\sigma^3 = 0.001$ ($\varphi = 0.052\%$) so that the susceptibility is comprised of noninteracting single-particle and cluster contributions. The dipolar coupling constant was varied in the range $1 \le \lambda \le 8$.

B. Brownian dynamics simulations of the dynamic magnetic susceptibility

BD simulations were carried out using LAMMPS [32, 33]. As explained in earlier work [16, 20, 34], this was achieved by using the Langevin-dynamics thermostat in LAMMPS, but with a high friction coefficient (or small damping time, t^*_damp) so that the inertial dynamics is suppressed after a sufficiently short time. In Lennard-Jones units, $t^*_\mathrm{damp} = 0.05$, corresponding to a Brownian rotation time of $\tau^*_\mathrm{B} = 1/6T^*t^*_\mathrm{damp} = 10/3$ [16]. BD simulations were carried out with $N = 4096$ particles, a time step $\delta t^* = 0.0025$, and the particle-particle particle-mesh implementation of the Ewald sum for dipolar interactions [35]. Equilibration took up to 2×10^7 time steps, and a typical production-run length was 1×10^7 time steps, corresponding to $7500\tau_\mathrm{B}$. 4 independent production runs were carried out for each system, and the results were averaged.

The static ($\omega = 0$) susceptibility was calculated using the formula

$$\chi(0) = \frac{\mu_0\langle M^2\rangle}{3Vk_\mathrm{B}T} \quad (3)$$

where $M = |\boldsymbol{M}|$ and $\boldsymbol{M} = \sum_{i=1}^N \boldsymbol{\mu}_i$. Linear response theory relates the decay of spontaneous magnetization fluctuations in the absence of a field, to the response function of the magnetization to a weak ac magnetic field (i.e., the initial susceptibility) [19]. The dynamic susceptibility $\chi(\omega)$ was thereby obtained from the Fourier transform of

the magnetization autocorrelation function $C(t)$ in zero field.

$$C(t) = \frac{\langle \boldsymbol{M}(t) \cdot \boldsymbol{M}(0) \rangle}{\langle M^2 \rangle} \tag{4a}$$

$$\frac{\chi(\omega)}{\chi(0)} = 1 + i\omega \int_0^\infty C(t) e^{i\omega t} dt \tag{4b}$$

With small values of λ, and a decay time in $C(t)$ on the order of τ_B, a direct numerical Fourier transform is sufficient. With large values of λ, the pronounced chaining, and concomitant slow decay and statistical noise of $C(t)$, give rise to particular problems in resolving the low-frequency dynamics. To get around this problem, $C(t)$ was fitted by a sum of exponential functions, and then $\chi(\omega)$ was obtained analytically. It was found that an effective fitting function was

$$C(t) = [(1 - f_0) + f_0 \exp(-t/\tau_0)] \sum_{j=1}^{n} f_j \exp(-t/\tau_j) \tag{5}$$

with the constraint $\sum_{j=1}^{n} f_j = 1$. The first factor was introduced to describe any initial rapid decay of the correlation function to a finite value $(1 - f_0)$ (shown in Section III B to arise from intracluster motions), while the second factor describes the ultimate, slow decay of the correlation function towards zero. If $f_0 = 0$, then there is a monotonic decay, while if $f_0 > 0$, there is a two-step relaxation process. The suitability of this function will be demonstrated in Section III B. Since $C(t)$ is just a sum of exponential functions, each term of the form $f \exp(-t/\tau)$ gives a contribution $f/(1 - i\omega\tau)$ to the dynamic susceptibility in Eq. (4b).

C. Theory of the static magnetic susceptibility

Increasing the dipolar coupling constant λ in the low-concentration ferrofluid causes complicated changes to the cluster distribution due to the balance of energy and entropy. Chains form in the region of $\lambda \gtrsim 4$ because the energetic benefit of the head-to-tail configuration of the dipolar particles outweighs the entropic cost of binding particles together, and so clustering minimises the free energy. In the region of $\lambda \gtrsim 7$, chains are the predominant structural units, and these can 'close up' to form rings, in order to gain the most energetic benefit, but at the cost of losing some conformational entropy. The structural transitions between free particles, chains, and rings can be described theoretically with the help of a classical density functional theory. In this theory, the system is modeled as an ideal mixture of noninteracting chains and ring-like clusters, which is appropriate to the very low concentration being considered in this work. The concentration of chains containing n particles is denoted by ρ_n^c, and that of rings by ρ_n^r. A free particle corresponds to a chain with $n = 1$. The Helmholtz free energy F is written as a functional of the concentrations of clusters [30].

$$\frac{F[\{\rho_n^\mathrm{c}\}, \{\rho_n^\mathrm{r}\}]}{V k_\mathrm{B} T} = \sum_{n=1}^{\infty} \rho_n^\mathrm{c} \ln\left(\frac{\rho_n^\mathrm{c} \mathcal{V}^n}{e Q_n^\mathrm{c}}\right) + \sum_{n=5}^{\infty} \rho_n^\mathrm{r} \ln\left(\frac{\rho_n^\mathrm{r} \mathcal{V}^n}{e Q_n^\mathrm{r}}\right) \tag{6}$$

Here, $\mathcal{V}$ is the de Broglie thermal volume of a single particle, and Q_n^c and Q_n^r are the temperature-dependent, internal partition functions of chain-like and ring-like clusters, respectively. Note that $Q_1^\mathrm{c} = 1$, and the ring contribution is limited to $n \geq 5$, on the basis that smaller rings are not observed in practice [26–29]. The cluster concentrations are constrained by the following conservation condition.

$$\sum_{n=1}^{\infty} n\rho_n^\mathrm{c} + \sum_{n=5}^{\infty} n\rho_n^\mathrm{r} = \rho \tag{7}$$

With high dipolar coupling constants, the clusters are rather long, and the internal partition functions of both chains and rings can be expressed in terms of the dimer partition function, q.

$$Q_n^\mathrm{c} = \sigma^{3(n-1)} \left(\frac{q}{\sigma^3}\right)^{C_n} \tag{8a}$$

$$C_n = \sum_{k=1}^{n} \frac{n-k}{k^3} \tag{8b}$$

$$Q_n^\mathrm{r} = \frac{\sigma^{3(n-1)}}{n^{1+3\nu}} \left(\frac{q}{\sigma^3}\right)^{R_n} \tag{8c}$$

$$R_n = \frac{n}{8} \sin^3\left(\frac{\pi}{n}\right) \sum_{k=1}^{n-1} \frac{\cos\left(\frac{2\pi k}{n}\right) + 3}{\sin^3\left(\frac{\pi k}{n}\right)} \tag{8d}$$

The exponent C_n takes into account the number and relative strength of interparticle interactions within a chain of n particles: the denominator k^3 reflects the cubic decrease of the dipole-dipole interaction energy with increasing separation along the chain. Note that $C_2 = 1$ and hence $Q_2^\mathrm{c} = q$. The exponent R_n is the exact sum of the relative interaction strengths of an ideal circular ring of n particles [36, 37], with the particle magnetic moments oriented at tangents to the circle. The denominator in Eq. (8c) takes into account (i) the n possible ways that a ring could be opened to form a chain with the same number of particles, and (ii) the entropy loss of changing a chain into a closed ring. The difference between the numbers of self-avoiding paths of a chain and a ring is proportional to $n^{3\nu}$ [38], where $\nu \approx 0.588$ is the Flory exponent for the self-avoiding random walk. The dimer partition function was calculated as for dipolar hard spheres with $\lambda \gg 1$ [39].

$$q = \frac{\sigma^3 e^{2\lambda}}{3\lambda^3} \left(1 + \frac{8}{3\lambda} + \frac{23}{3\lambda^2} + \ldots\right) \tag{9}$$

Minimization of the free energy functional (6) with the conservation condition (7), gives the chain and ring concentrations as powers of the activity $z = \exp(\Lambda)/\mathcal{V}$,

where Λ is the Lagrange multiplier, which is proportional to the chemical potential.

$$\rho_n^{\rm c} = Q_n^{\rm c} z^n \tag{10a}$$

$$\rho_n^{\rm r} = Q_n^{\rm r} z^n \tag{10b}$$

z is found by substituting (10) into (7).

To calculate the static magnetic properties of the clustered dipolar fluid, it is assumed that the total magnetic moment of a ring-like cluster is equal to zero, since the magnetic flux is closed inside the cluster. So, all magnetic particles bonded in rings are considered as 'magnetic holes' which do not contribute to the static susceptibility of the system. The magnetic response of a flexible n-particle chain is determined by the reduced mean-squared magnetic moment $\langle m_n^2 \rangle$ [39, 40].

$$\langle m_n^2 \rangle = n + \frac{2\kappa\left(n - 1 + \kappa^n - n\kappa\right)}{\left(1-\kappa\right)^2} \tag{11a}$$

$$\kappa \approx \coth\left(\frac{\lambda}{2}\right) - \frac{2}{\lambda} \tag{11b}$$

The correlation coefficient $0 \le \kappa \le 1$ describes the projection of a magnetic moment onto its neighbors in the chain, and so it is a measure of chain flexibility. The simple analytical expression for κ is an approximation, and was derived for dipolar hard spheres in Ref. 39. The limit $\kappa \to 0$ corresponds to a complete loss of orientational correlations between neighboring particles in the chain, and hence $\langle m_n^2 \rangle \to n$, as for a random walk. The opposite limit corresponds to perfect alignment of the particles in the chain, and in this case, $\langle m_n^2 \rangle \to n^2$. Hence, the magnetic response of an inflexible chain (with large λ) is much greater than that of a flexible chain (with small λ). The static susceptibility is given by

$$\chi(0) = \left(\frac{4\pi\lambda}{3}\sum_{n=1}^{\infty}\rho_n^{\rm c}\sigma^3\langle m_n^2\rangle\right)\left(1 + \frac{1}{3}\chi_{\rm L}^{\rm c}\right) \tag{12}$$

where $\chi_{\rm L}^{\rm c} = (4\pi\lambda/3)\sum_{n=1}^{\infty}\rho_n^{\rm c}\sigma^3$ is the Langevin susceptibility of all particles that are aggregated into chains. The first factor is basically the Langevin susceptibility of the ideal gas of chains, while the second factor is a modification to take account of the interaction between each chain and the mean field arising from all other particles in chains [41]; recall that particles in rings are considered as magnetic holes. In the limit $\lambda \to 0$, there are only free particles, and with $\rho_1^{\rm c} = \rho$, $\langle m_1^2 \rangle = 1$, and $\chi_{\rm L}^{\rm c} = 4\pi\lambda\rho\sigma^3/3$, the static susceptibility is $\chi(0) = \chi_{\rm L}^{\rm c}(1 + \chi_{\rm L}^{\rm c}/3)$, which is the familiar, first-order modified mean field theory result [41].

III. RESULTS

A. Static susceptibility

The ratio of the static susceptibility and the Langevin susceptibility is plotted as a function of λ in Fig. 1(a).

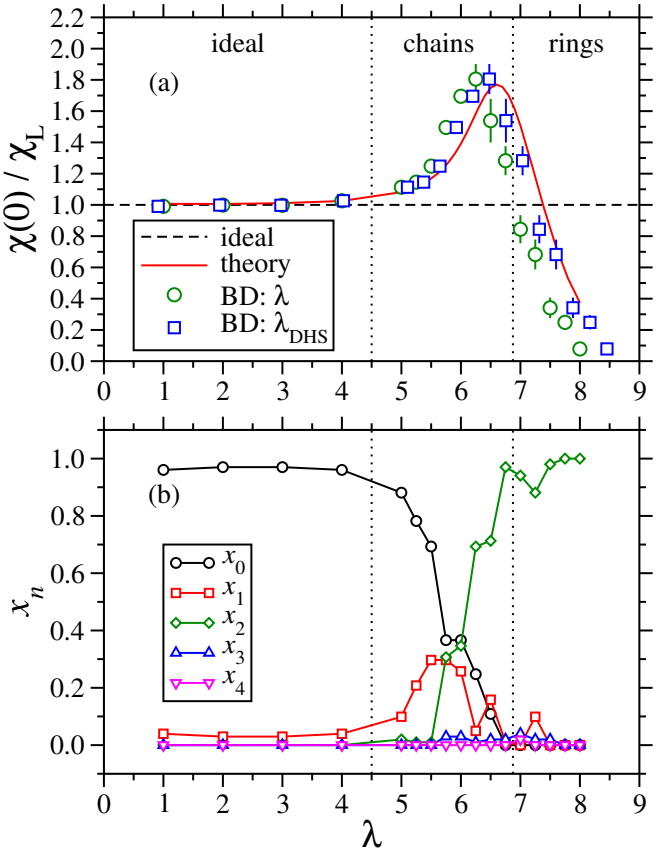

FIG. 1. (a) The static susceptibility $\chi(0)$ divided by the Langevin susceptibility $\chi_{\rm L}$, as a function of the dipolar coupling constant λ, for fluids with reduced concentration $\rho\sigma^3 = 0.001$. The green-dashed line is for non-interacting particles, the red line is from Eq. (12), and the points are from BD simulations with the nominal and effective DHS values of the dipolar coupling constant. (b) The fractions of particles with 0, 1, 2, 3, and 4 nearest neighbors as a function of λ. In (a) and (b), the black dotted lines are approximate boundaries between states where the structure is primarily unclustered particles, chains, and rings.

The Langevin susceptibility $\chi_{\rm L} = 4\pi\rho\sigma^3\lambda/3$ is the result for noninteracting particles. Figure 1(b) shows the fractions of particles with 0, 1, 2, 3, and 4 neighbors, based on a distance criterion with a cutoff equal to the position of the first minimum in the function $r^2 g(r)$, where $g(r)$ is the radial distribution function (not shown). The cutoff distance varied from 1.6σ at $\lambda = 1$, to 1.3σ at $\lambda = 8$.

The results in Fig. 1(a) are exactly in line with earlier work [30]. Below $\lambda \simeq 5$, the static susceptibility is very close to the Langevin susceptibility, suggesting that the system is comprised of weakly interacting particles. This is supported by the simulation snapshot in Fig. 2(a), and the observation that $x_0 \simeq 1$ [Fig. 1(b)].

The static susceptibility shows an enhancement in the range $5 \le \lambda \le 6.75$, which is due to the formation of chains, as exemplified by the simulation snapshot in Fig. 2(b). Over this range of λ, x_2 rises from zero to

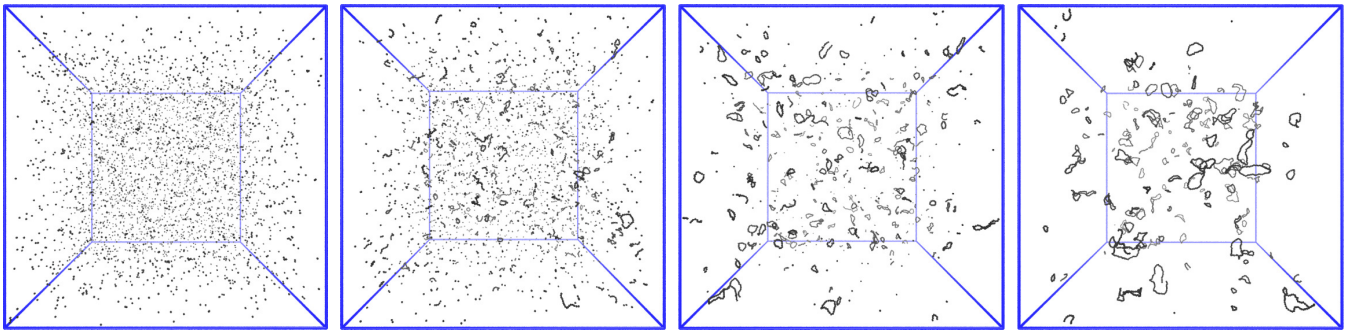

FIG. 2. Simulation snapshots for systems with reduced concentration $\rho\sigma^3 = 0.001$ and dipolar coupling constants (a) $\lambda = 5$, (b) $\lambda = 6$, (c) $\lambda = 7$, and (d) $\lambda = 8$.

close to one, corresponding to the internal particles in the chains, while x_1 is small but non-zero, corresponding to the particles at the ends of chains. Chains of aligned particles possess large, net dipole moments, and these give large contributions to the magnetization fluctuations. Note that the chains are not very long in this regime. Roughly speaking, extensive aggregation is expected when $\rho q \gtrsim 1$, and using Eq. (9), this should occur at $\rho\sigma^3 \gtrsim 0.0093$ with $\lambda = 5$, and $\rho\sigma^3 \gtrsim 0.00081$ with $\lambda = 6.75$. This explains the lack of very long chains in Fig. 2(a) and (b). Using the same distance-based criterion as for the calculation of x_n, the average cluster size is $\langle n \rangle = 1.1$ with $\lambda = 5$, and $\langle n \rangle = 2.0$ with $\lambda = 6$. For similar values of λ, and with increasing concentration, the chains increase in length, overlap to form a network-like structure, and ultimately disappear as the structure crosses over to that of a typical dense liquid [21–24].

In the range $\lambda \geq 7$, the number of rings grows significantly, and since the net dipole moments are very much smaller due to flux closure, the static susceptibility drops rapidly as chains transform into rings. The snapshots in Fig. 2(c) and (d) illustrate this transformation. The average cluster size is $\langle n \rangle = 10.4$ with $\lambda = 7$, and $\langle n \rangle = 26.9$ with $\lambda = 8$. With these high values of λ, x_1 is practically zero, x_2 is close to one, and the small values of x_3 and x_4 signal the occasional occurrence of Y- and X-shaped defects [26–29, 42].

On the basis of these three ranges, boundaries between states dominated by unclustered particles, chains, and rings are placed in Fig. 1 at $\lambda = 4.5$ and $\lambda = 6.875$. The full cluster distributions, and the contributions to the static susceptibility from particles, chains, and rings have been studied in detail in previous theoretical and simulation work [30]. For the specific concentration studied in this work, the theoretical prediction outlined in Section II C is shown in Fig. 1(a). The theoretical and simulation results are qualitatively the same, although the theoretical curve is shifted to higher values of λ. The reason for this is that the theoretical model is based on a hard-sphere short-range potential, while the BD simulations employ a soft, WCA potential. Since the WCA particles are able to get closer than the nominal diameter σ, the effective dipolar coupling constant is higher than nominal value λ. To obtain a mapping between the hard-sphere and WCA variants, the respective dipolar coupling constants are related by equating the two-particle partition functions, where the particles are aligned in the ground-state, nose-to-tail conformation. The partition function q is effectively a dimerization equilibrium constant, and so this should provide a reasonable basis for a mapping between the two systems.

$$\begin{aligned} q &= \int_0^\infty r^2 \exp\left[-\frac{u^{\mathrm{WCA}}(r)}{k_{\mathrm{B}}T} + 2\lambda\left(\frac{\sigma}{r}\right)^3\right] dr \\ &= \int_\sigma^\infty r^2 \exp\left[2\lambda_{\mathrm{DHS}}\left(\frac{\sigma}{r}\right)^3\right] dr \end{aligned} \tag{13}$$

Here λ is the dipolar coupling constant used in simulations, λ_{DHS} is the effective dipolar hard sphere (DHS) value, and the lower limit of the second integration arises from the hard-sphere potential. Of course, these integrals do not converge due to the $(\sigma/r)^3$ factor in the dipolar interaction, but by writing $r = \sigma(1 + x)$ with x being small [43], this factor is approximated by $1 - 3x$, which is justified for strongly clustered particles in close contact. With this approximation, the integrals converge, and for each value of λ used in the BD simulations, it is possible to find a value of λ_{DHS} which should give rise to a similar extent of clustering. (Some example values are given in Table I.) In Fig. 1(a), the BD results are shown as a function of λ_{DHS}, and as anticipated, this brings the results closer to the DHS theory. Overall, the physical picture detailed in previous work [30] corresponds well with the current simulation results and implementation of the theory.

B. Dynamic susceptibility

Examples of the magnetization autocorrelation function are shown in Fig. 3. These examples illustrate the gamut of behaviors seen in simulations. In each case, the

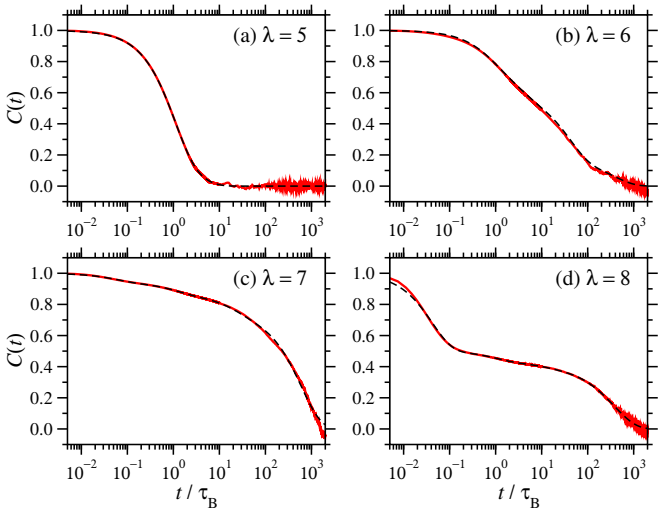

FIG. 3. The magnetization autocorrelation function $C(t)$ for fluids with reduced concentration $\rho\sigma^3 = 0.001$: (a) $\lambda = 5$; (b) $\lambda = 6$; (c) $\lambda = 7$; (d) $\lambda = 8$. The solid red line shows the raw BD simulation data, and the dashed black line is a fit using Eq. (5).

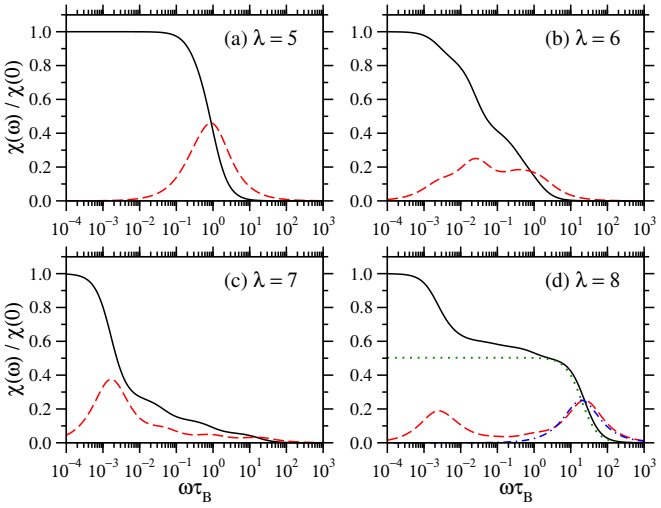

FIG. 4. The dynamic susceptibility $\chi(\omega)$ divided by the static susceptibility $\chi(0)$ for fluids with reduced concentration $\rho\sigma^3 = 0.001$: (a) $\lambda = 5$; (b) $\lambda = 6$; (c) $\lambda = 7$; (d) $\lambda = 8$. The solid black line is the real part $\chi'(\omega)$, and the dashed red line is the imaginary part $\chi''(\omega)$. In (d), the dotted green line and the dot-dashed blue line are, respectively, the real and imaginary parts of the Debye function with an effective relaxation time $\tau_{\rm eff} = 0.0510\tau_{\rm B}$, scaled to give the correct peak height in χ''.

raw simulation results and multiexponential fits (5) are shown. With $\lambda = 5$, $C(t)$ looks like a single-exponential decay. With $\lambda = 6$ and 7, the decays are orders of magnitude slower, and more complex in character; these results required $f_0 > 0$ and $n = 3$ in Eq. (5) to get a good fit. With $\lambda = 8$, there is a clear, two-step relaxation process, and $f_0 > 0$ and $n = 4$ gave an adequate fit. Figure 3 shows that the fitted functions are faithful representations of the simulation results.

Examples of the dynamic susceptibility are shown in Fig. 4, for the same values of λ just discussed. With $\lambda = 5$, there is a single peak in χ'' in the region of $\omega = \tau_{\rm B}^{-1}$. The detailed dependence of the peak frequency on the dipolar coupling constant in the weakly interacting regime was studied theoretically and with simulations in earlier work [16, 20]. The dynamic response is essentially that of interacting but unclustered particles.

With $\lambda = 6$, two clear peaks in χ'' are in evidence: one at $\omega\tau_{\rm B} \simeq 0.0258$, and the other at $\omega\tau_{\rm B} \simeq 0.395$. The obvious interpretation is that the lower frequency peak arises from short chains, and the higher frequency peak arises from unclustered, but interacting particles.

With $\lambda = 7$, the predominant peak in χ'' is at $\omega\tau_{\rm B} \simeq 0.00168$, which again must be due to chains, but now longer ones. There are other features at frequencies of $\omega\tau_{\rm B} \sim 0.1$, 1, and 10. The lower frequency features must be due to short chains and unclustered particles, while the higher frequency feature will be linked explicitly to motions within long chains and rings (see Section III C). The snapshot in Fig. 2(c) shows that there are rings, chains, and unclustered particles in coexistence. The unclustered particles obviously contribute significantly to the magnetization fluctuations, but not as much as chains, since the latter carry larger net dipole moments. The ground-state (lowest-energy) conformation of a ring has no net dipole moment. Hence, the chain contribution to $\chi(\omega)$ is absolutely dominant. But there will also be high-frequency motions of particles within long-lived chains and rings, which will make small contributions to the relaxation of spontaneous magnetization fluctuations. These fluctuations give rise to the weak high-frequency features in $\chi(\omega)$.

With $\lambda = 8$, the number of chains is lower, and the number of rings is higher. Hence, the high-frequency peak in χ'' should become more visible, and that is exactly what is shown in Fig. 4. Figure 2(d) shows an almost total absence of unclustered particles, and hence χ'' no longer exhibits intermediate-frequency features. The peak at low frequency $\omega\tau_{\rm B} \simeq 0.00250$ is due to a small number of long chains, while the peak at high frequency $\omega\tau_{\rm B} \simeq 23.7$ is due to motions within chains and rings.

The out-of-phase, imaginary part of the dynamic susceptibility is summarized for all systems using a heat map, shown in Fig. 5. To cancel out the variation in the magnitude of the susceptibility, $\chi''(\omega)$ for each value of λ is divided by its maximum value. Therefore, the heat map represents the distribution of response times, and not the magnitude of the response, which is largely dictated by $\chi(0)$. The heat map shows three distinct regimes. With $\lambda \leq 5.5$, there is just one peak in the region of $\omega\tau_{\rm B} \simeq 1$, and so this is the single-particle regime. In the range $5.75 \leq \lambda \leq 6.75$, as the single-particle feature diminishes with increasing λ, a low-frequency feature emerges due to the rotational dynamics of chains; therefore, this crossover represents a mixed

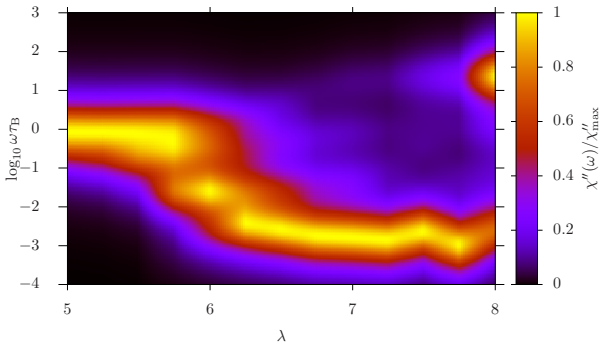

FIG. 5. Heat map showing $\chi''(\omega)/\chi''_{\max}$ from BD simulations, as a function of λ and $\log_{10}\omega\tau_B$ for fluids with reduced concentration $\rho\sigma^3 = 0.001$. $\chi''_{\max}$ is the maximum value of χ'' for a given value of λ.

single-particle/chain regime. Finally, with $\lambda \geq 7$, a new high-frequency feature emerges, and as explained above, there are two characteristic timescales in this chain/ring regime; the low-frequency feature arises from chain rotations, and the high-frequency feature arises from particle motions within chains and rings.

The peak frequencies and peak heights in $\chi''(\omega)$ are plotted in Fig. 6 as functions of λ. Figure 6(a) shows that the peak frequencies ($\omega_{\max}$) can be conveniently divided into three groups: peak 1 represents largely free particles and short chains; peak 2 represents long chains; and peak 3 represents motions within chains and rings. This division is less clear around $\lambda = 5.75$ and 6.00, but the overall progression with increasing λ is plausible, and the loci of peaks 1 and 2 are reminiscent of an order parameter for a phase transition, although none exists here. The high-frequency peaks at $\lambda \geq 7$ are explained quantitatively in Section III C, and Fig. 6(a) shows the theoretical predictions explained therein.

Figure 6(b) shows the peak heights ($\chi''_{\max}$) relative to the static susceptibility $\chi(0)$. In the ideal regime, $\chi''_{\max} = \chi(0)/2$, as per the prediction of the simple Debye theory. In the chain regime, this peak contribution drops, and the peak-2, chain contribution grows. Finally, in the ring regime, the peak-2 contribution begins to drop, and the peak-3 contribution grows. These results show that, in the chain and ring regimes, there is a spread of contributions with different weights and characteristic frequencies, which reflects the coexistence of various clusters.

C. High-frequency peak in χ''

Figure 6(a) shows that with $\lambda \geq 7$, there is a high-frequency peak in χ'' with $\omega_{\max}\tau_B = 15$–24. The precise values are presented in Table I. The hypothesis is that the high-frequency peak arises from single-particle motions within clusters, under the influence of the local magnetic field arising from its neighbors. To develop a theory, it is sufficient to consider a chain only, even though its dynamic response is dominated by the rotation of the chain as a whole. The dynamics within a ring will be very similar, but of course it has no net dipole moment, and so its response will be dominated by its internal dynamics, at least on a short time scale. On longer time scales, fluctuations in the ring shape, opening into chains, and exchanges of particles between clusters will come into effect.

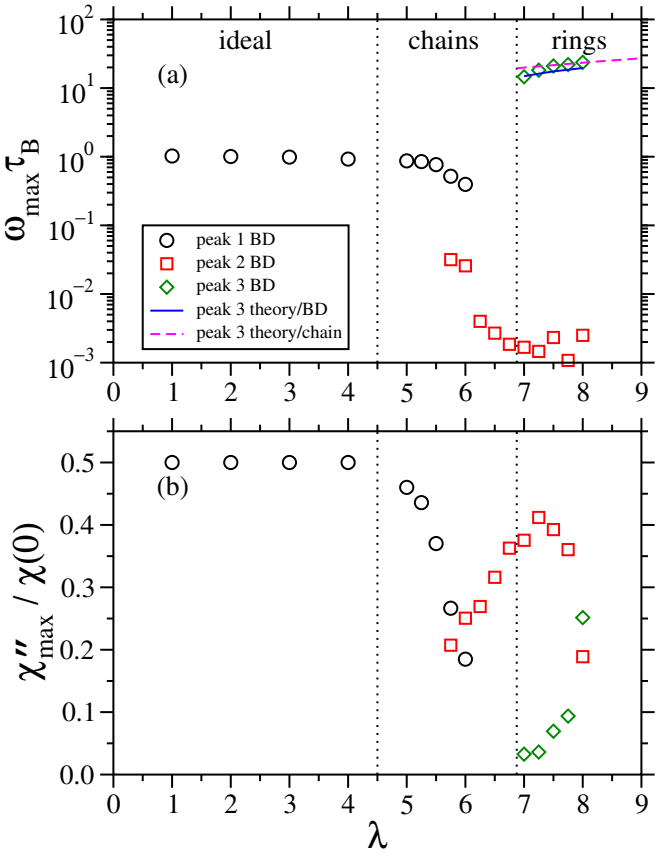

FIG. 6. Peak positions (a) and peak heights (b) in $\chi''(\omega)/\chi(0)$ for fluids with reduced concentration $\rho\sigma^3 = 0.001$. The peaks are separated into three arbitrarily labeled groups (1, 2, and 3), with peak 1 representing motions of unclustered particles, peak 2 representing motions of chains, and peak 3 representing motions within chains and rings. In (a), the solid blue and dashed magenta lines are, respectively, the theory/BD and theory/chain predictions given by Eq. (26), as detailed in Section III C. In (b), the peak heights $\chi''_{\max}$ are plotted relative to the static susceptibility $\chi(0)$.

So, consider a single particle in a linear chain, in which the magnetic dipole moments are preferentially aligned in the same direction. The chain orientation is parallel to the laboratory z axis. The local magnetic field arising from all of the other particles is $\boldsymbol{H} = (0, 0, H)$. It is convenient to consider motion of the chosen particle's dipole moment in a local xz plane, so that the $\boldsymbol{\mu} = \mu\boldsymbol{u}$, and $\boldsymbol{u} = (\sin\theta, 0, \cos\theta)$ is a unit orientation vector. The

TABLE I. Properties of fluids with reduced concentration $\rho\sigma^3 = 0.001$, relevant to the calculation of the high-frequency peak position in $\chi''(\omega)$. U is the dipolar energy per particle, $K = -2U$ is the corresponding mean field, and $\omega_{\max}$ is the position of the high-frequency maximum in $\chi''(\omega)$. The results labeled ''BD' are purely from the BD simulations. The results labeled 'theory/BD' are obtained using Eq. (26) and the BD values of U and K. The results labeled 'theory/chain' are for an infinite chain of particles in its ground-state configuration. $\lambda_{\rm DHS}$ is the solution of Eq. (13).

λ	$\lambda_{\rm DHS}$	$U/k_{\rm B}T$	$K/k_{\rm B}T$	$\omega_{\max}\tau_{\rm B}$	Source
7.00	7.32	−14.9	29.7	14.6	BD
				14.9	theory/BD
		−19.9	39.7	19.9	theory/chain
7.25	7.60	−16.2	32.5	18.2	BD
				16.2	theory/BD
		−20.7	41.5	20.7	theory/chain
7.50	7.88	−17.5	34.9	21.0	BD
				17.5	theory/BD
		−21.6	43.3	21.6	theory/chain
7.75	8.17	−18.5	37.0	22.0	BD
				18.5	theory/BD
		−22.5	45.1	22.5	theory/chain
8.00	8.45	−19.6	39.2	23.7	BD
				19.6	theory/BD
		−23.4	46.8	23.4	theory/chain

Langevin equation in the overdamped limit is

$$\dot{\boldsymbol{L}} = -\gamma\dot{\boldsymbol{\omega}} + \boldsymbol{F} + \boldsymbol{R} = 0 \tag{14}$$

where $\boldsymbol{L}$ is the angular momentum, γ is a friction coefficient, $\boldsymbol{\omega}$ is the angular velocity, $\boldsymbol{F}$ is the torque arising from the local magnetic field, and $\boldsymbol{R}$ is the random Brownian torque arising from the suspending liquid. The friction coefficient is related to the rotational diffusion coefficient and the Brownian rotation time by $\gamma = k_{\rm B}T/D = 2k_{\rm B}T\tau_{\rm B}$. The torque from the local field is

$$\boldsymbol{F} = \mu_0\left(\boldsymbol{\mu}\wedge\boldsymbol{H}\right) = -K(0,\sin\theta,0) \tag{15}$$

where $K = \mu_0\mu H$ has units of energy. The statistics of the random torques in any given direction are given by the usual relations

$$\langle R(t)\rangle = 0, \tag{16a}$$
$$\langle R(t)R(t')\rangle = 2\gamma k_{\rm B}T\delta(t-t'). \tag{16b}$$

With these specifications, the Brownian rotational dynamics of the particle are given by

$$-\gamma\frac{d\theta}{dt} - K\sin\theta + R = 0. \tag{17}$$

When the magnetic particles are strongly associated and aligned in chains, the deviations from perfect alignment are small. It is therefore sufficient to consider the approximate equation

$$-\gamma\frac{d\theta}{dt} - K\theta + R = 0 \tag{18}$$

which has a simple solution given by

$$\theta(t) = \theta(0)e^{-Kt/\gamma} + \frac{1}{\gamma}e^{-Kt/\gamma}\int_0^t R(t_1)e^{Kt_1/\gamma}dt_1. \tag{19}$$

The single-particle motions should give a contribution to $C(t)$ of the form

$$\begin{aligned}\langle\boldsymbol{u}(t)\cdot\boldsymbol{u}(0)\rangle &= \langle\sin\theta(t)\sin\theta(0) + \cos\theta(t)\cos\theta(0)\rangle \\ &= \langle\cos\Delta\theta(t)\rangle \approx 1 - \frac{1}{2}\left\langle\Delta\theta^2(t)\right\rangle\end{aligned} \tag{20}$$

where $\Delta\theta(t) = \theta(t) - \theta(0)$. At long times, $\langle\theta(t)\theta(0)\rangle \to 0$ and hence $\langle\Delta\theta^2(t)\rangle \to 2\langle\theta^2\rangle$. From Eqs. (16a), (16b), and (19)

$$\left\langle\Delta\theta^2(t)\right\rangle = \left\langle\theta^2\right\rangle\left(1 - e^{-Kt/\gamma}\right)^2 + \frac{k_{\rm B}T}{K}\left(1 - e^{-2Kt/\gamma}\right). \tag{21}$$

The aforementioned long-time limit implies that $k_{\rm B}T = K\langle\theta^2\rangle$, as per the equipartition theorem. The final result is therefore

$$\langle\boldsymbol{u}(t)\cdot\boldsymbol{u}(0)\rangle = 1 - \left\langle\theta^2\right\rangle\left(1 - e^{-Kt/\gamma}\right). \tag{22}$$

This shows that the correlation function decays to a finite value of $1 - \langle\theta^2\rangle$, because the dipole moments are aligned within the chain. In the small-K limit, the short-time dynamics are described by

$$\langle\boldsymbol{u}(t)\cdot\boldsymbol{u}(0)\rangle \approx 1 - \left(\frac{K\langle\theta^2\rangle}{\gamma}\right)t = 1 - Dt \tag{23}$$

$$\left\langle\left[\boldsymbol{u}(t) - \boldsymbol{u}(0)\right]^2\right\rangle = 2 - 2\langle\boldsymbol{u}(t)\cdot\boldsymbol{u}(0)\rangle \approx 2Dt \tag{24}$$

confirming that the rotational diffusion constant is $D = k_{\rm B}T/\gamma = 1/2\tau_{\rm B}$. Equation (22) therefore shows that, in the presence of a field, the initial decay is governed by an effective time scale

$$\tau_{\rm eff} = \frac{\gamma}{K} = \left(\frac{2k_{\rm B}T}{K}\right)\tau_{\rm B} \tag{25}$$

and hence the position of the maximum in $\chi''(\omega)$ should be

$$\omega_{\max}\tau_{\rm B} = \frac{\tau_{\rm B}}{\tau_{\rm eff}} = \frac{K}{2k_{\rm B}T}. \tag{26}$$

The dipolar interaction energy per particle, U, can be obtained directly from the BD simulations, and identifying the interaction between a dipole and the local field gives $K = -2U$. These data are listed in Table I for $7 \le \lambda \le 8$, along with $\omega_{\max}$ extracted directly from $\chi''(\omega)$ (labeled 'BD'), and from Eq. (26) using the BD value for K (labeled 'theory/BD'). The agreement between BD simulation results and Eq. (26) is satisfactorily close: the results are compared in Fig. 6(a). The corresponding Debye functions with the effective relaxation time $\tau_{\rm eff} = 0.0510\tau_{\rm B}$ (25) and the same peak height in χ'' are shown for $\lambda = 8$ in Fig. 4(d).

Purely theoretical predictions can be obtained for the ground-state configuration of an infinite linear chain of particles, with perfectly aligned dipole moments, interacting via the WCA and dipole-dipole potentials, and with $T^* = 1$. In this case, the ground-state separation r_0 of the particles minimises the function

$$\frac{u^{\mathrm{WCA}}(r)}{k_{\mathrm{B}}T} - 2\lambda\left(\frac{\sigma}{r}\right)^3 \tag{27}$$

and the dipolar energy per particle is $U/k_{\mathrm{B}}T = -2\zeta(3)\lambda/r_0^3$, where $\zeta(3) \simeq 1.202$ is Apéry's constant. Using the same arguments as above gives the values of U, K, and $\omega_{\max}$ labeled 'theory/chain' in Table I. The values of $\omega_{\max}$ are plotted in Fig. 6 for comparison with the BD and theory/BD results, showing good consistency between the different approaches. The theory/BD approach is slightly better near $\lambda = 7$, and the theory/chain approach is slightly better near $\lambda = 8$, but the differences are not very significant.

Equation (25) is qualitatively consistent with the relaxation of the magnetization parallel to a uniform external field (H_{ext}) in an ideal system of non-interacting particles [17, 44, 45]. There is a spectrum of relaxation times, the longest of which is [44, 45]

$$\tau_{\mathrm{eff}} = \left[\frac{\alpha L_1(\alpha)}{L(\alpha)}\right]\tau_{\mathrm{B}} \tag{28}$$

where $\alpha = \mu_0\mu H_{\mathrm{ext}}/k_{\mathrm{B}}T$ is the Langevin parameter, $L(\alpha) = \coth\alpha - 1/\alpha$ is the Langevin function, and $L_1(\alpha) = dL/d\alpha$. In the strong-field limit, this becomes $\tau_{\mathrm{eff}} \approx \tau_{\mathrm{B}}/\alpha$, and so with α being analogous to $K/2k_{\mathrm{B}}T$, the results are similar. Essentially, a local magnetic field parallel to the dipole orientation decreases the relaxation time.

IV. CONCLUSIONS

Cluster formation in low-concentration, strongly interacting ferrofluids has been shown to have profound effects on the frequency-dependent, dynamic susceptibility. With increasing interaction strength, the structural motifs of the system progress from free particles, through chain-like clusters, to ring-like clusters. The impact of this progression on the static susceptibility is already known [30], and the present results agree well with earlier work. Each of the motifs has its own characteristic relaxation timescale, which manifests itself in distinct features in the dynamic susceptibility. Free particles have relaxation times that do not deviate significantly from the Brownian rotation time. Chain-like clusters rotate only very slowly, and so low-frequency features emerge in the dynamic susceptibility. The contributions from particle motions within chains and rings become apparent once chains close up to form rings, and these give rise to features in the high-frequency dynamic susceptibility due to the effects of the local magnetic fields within the clusters. The high-frequency features can be captured quantitatively using a simple mean-field, Brownian-dynamical equation of motion.

This study was confined to very low concentration ferrofluids, so that the distinct contributions from different clusters could be clearly discerned. An obvious extension is to study more concentrated systems with strong interactions, where gel-like structures are to be anticipated [46–49]. On the one hand, $\chi(\omega)$ may still show the high-frequency features arising from particle motions within self-assembled structures. On the other hand, gel-like structures could undergo extremely slow relaxation, which may be out of reach of simulation. Work on this regime is in progress.

ACKNOWLEDGMENTS

A. O. I. gratefully acknowledges research funding from the Ministry of Science and Higher Education of the Russian Federation (Ural Mathematical Center Project No. 075-02-2021-1387).

[1] R. E. Rosensweig, *Ferrohydrodynamics* (Dover Publications, Inc., New York, 1998).
[2] R. E. Rosensweig, J. Mag. Magn. Mater. **252**, 370 (2002).
[3] Q. A. Pankhurst, J. Connolly, S. K. Jones, and J. Dobson, J. Phys. D: Appl. Phys. **36**, R167 (2003).
[4] Q. A. Pankhurst, N. T. K. Thanh, S. K. Jones, and J. Dobson, J. Phys. D: Appl. Phys. **42**, 224001 (2009).
[5] R. Hergt, R. Hiergeist, I. Hilger, W. Kaiser, Y. Lapatnikov, S. Margel, and U. Richter, J. Magn. Magn. Mater. **270**, 345 (2004).
[6] F. Sonvico, S. Mornet, S. Vasseur, C. Dubernet, D. Jaillard, J. Degrouard, J. Hoebeke, E. Duguet, P. Colombo, and P. Couvreur, Bioconjug. Chem. **16**, 1181 (2005).
[7] J.-P. Fortin, C. Wilhelm, J. Servais, C. Ménager, J.-C. Bacri, and F. Gazeau, J. Am. Chem. Soc. **129**, 2628 (2007).
[8] R. Müller, R. Hergt, M. Zeisberger, and W. Gawalek, J. Mag. Magn. Mater. **289**, 13 (2005).
[9] Yu. L. Raikher and V. I. Stepanov, J. Mag. Magn. Mater. **368**, 421 (2014).
[10] M. Boskovic, G. F. Goya, S. Vranjes-Djuric, N. Jovic, B. Jancar, and B. Antic, J. Appl. Phys. **117**, 103903 (2015).
[11] P. Ilg, Phys. Rev. E **100**, 022608 (2019).
[12] A. O. Ivanov, V. S. Zverev, and S. S. Kantorovich, Soft Matter **12**, 3507 (2016).

[13] A. O. Ivanov, S. S. Kantorovich, V. S. Zverev, E. A. Elfimova, A. V. Lebedev, and A. F. Pshenichnikov, Phys. Chem. Chem. Phys. **18**, 18342 (2016).

[14] A. O. Ivanov, S. S. Kantorovich, V. S. Zverev, A. V. Lebedev, A. F. Pshenichnikov, and P. J. Camp, J. Mag. Magn. Mater. **459**, 252 (2018).

[15] A. V. Lebedev, V. I. Stepanov, A. A. Kuznetsov, A. O. Ivanov, and A. F. Pshenichnikov, Phys. Rev. E **100**, 032605 (2019).

[16] J. O. Sindt, P. J. Camp, S. S. Kantorovich, E. A. Elfimova, and A. O. Ivanov, Phys. Rev. E **93**, 063117 (2016).

[17] T. M. Batrudinov, Yu. E. Nekhoroshkova, E. I. Paramonov, V. S. Zverev, E. A. Elfimova, A. O. Ivanov, and P. J. Camp, Phys. Rev. E **98**, 052602 (2018).

[18] A. Pshenichnikov, A. Lebedev, and A. O. Ivanov, Nanomaterials **9**, 1711 (2019).

[19] J.-P. Hansen and I. R. McDonald, *Theory of Simple Liquids*, 3rd ed. (Academic Press, London, 2006).

[20] A. O. Ivanov and P. J. Camp, Phys. Rev. E **98**, 050602(R) (2018).

[21] J. J. Weis and D. Levesque, Phys. Rev. Lett. **71**, 2729 (1993).

[22] D. Levesque and J. J. Weis, Phys. Rev. E **49**, 5131 (1994).

[23] M. J. Stevens and G. S. Grest, Phys. Rev. E **51**, 5962 (1995).

[24] P. J. Camp and G. N. Patey, Phys. Rev. E **62**, 5403 (2000).

[25] M. Klokkenburg, R. P. A. Dullens, W. K. Kegel, B. H. Erné, and A. P. Philipse, Phys. Rev. Lett. **96**, 037203 (2006).

[26] L. Rovigatti, J. Russo, and F. Sciortino, Phys. Rev. Lett. **107**, 237801 (2011).

[27] L. Rovigatti, J. Russo, and F. Sciortino, Soft Matter **8**, 6310 (2012).

[28] S. S. Kantorovich, A. O. Ivanov, L. Rovigatti, J. M. Tavares, and F. Sciortino, Phys. Chem. Chem. Phys. **17**, 16601 (2015).

[29] M. Ronti, L. Rovigatti, J. M. Tavares, A. O. Ivanov, S. S. Kantorovich, and F. Sciortino, Soft Matter **13**, 7870 (2017).

[30] S. Kantorovich, A. O. Ivanov, L. Rovigatti, J. M. Tavares, and F. Sciortino, Phys. Rev. Lett. **110**, 148306 (2013).

[31] A. Sreekumari and P. Ilg, Phys. Rev. E **88**, 042315 (2013).

[32] LAMMPS Molecular Dynamics Simulator, `http://lammps.sandia.gov` (2020).

[33] S. Plimpton, J. Comp. Phys. **117**, 1 (1995).

[34] A. O. Ivanov and P. J. Camp, Phys. Rev. E **102**, 032610 (2020).

[35] J. J. Cerdà, V. Ballenegger, O. Lenz, and C. Holm, J. Chem. Phys. **129**, 234104 (2008).

[36] T. A. Prokopieva, V. A. Danilov, S. S. Kantorovich, and C. Holm, Phys. Rev. E **80**, 031404 (2009).

[37] R. Messina, L. A. Khalil, and I. Stanković, Phys. Rev. E **89**, 011202(R) (2014).

[38] J. P. Wittmer, P. van der Schoot, A. Milchev, and J. L. Barrat, J. Chem. Phys. **113**, 6992 (2000).

[39] K. I. Morozov and M. I. Shliomis, Magnetic fluid as an assembly of flexible chains, in *Ferrofluids: Magnetically Controllable Fluids and Their Applications*, edited by S. Odenbach (Springer Berlin Heidelberg, Berlin, Heidelberg, 2002) pp. 162–184.

[40] V. S. Mendelev and A. O. Ivanov, Phys. Rev. E **70**, 051502 (2004).

[41] A. O. Ivanov and O. B. Kuznetsova, Phys. Rev. E **64**, 041405 (2001).

[42] T. Tlusty and S. A. Safran, Science **290**, 1328 (2000).

[43] P. C. Jordan, Mol. Phys. **25**, 961 (1973).

[44] M. A. Martsenyuk, Yu. L. Raikher, and M. I. Shliomis, Sov. Phys. JETP **38**, 413 (1974).

[45] M. I. Shliomis and Yu. L. Raikher, IEEE Trans. Magn. **16**, 237 (1980).

[46] P. Ilg and E. Del Gado, Soft Matter **7**, 163 (2010).

[47] D. A. Martin, T. S. Grigera, and V. I. Marconi, Phys. Rev. E **99**, 022604 (2019).

[48] M. Brito, M. A. Carignano, and V. Marconi, Sci. Rep. **10**, 3971 (2020).

[49] L. F. Elizondo-Aguilera, E. C. Cortés-Morales, P. F. Zubieta Rico, M. Medina-Noyola, R. Castañeda-Priego, T. Voigtmann, and G. Pérez-Ángel, Soft Matter **16**, 170 (2020).